Journal of Dynamics, Monitoring and Diagnostics, 2025, 4, 213-225
https://doi.org/10.37965/jdmd.2024.732

ISTP
RESEARCH ARTICLE

Investigating Thermal and Charge Rate Effects on Electric Vehicle Battery Degradation

Namrata Mohanty, Neeraj Kumar Goyal, and V N Achutha Naikan
Subir Chowdhury School of Quality and Reliability, Indian Institute of Technology Kharagpur, Kharagpur, West Bengal, India

(Received 09 January 2025; Revised 10 March 2025; Accepted 15 April 2025; Published online 15 April 2025)

Abstract: Electric vehicles (EVs) operate under diverse environmental conditions and charging scenarios, leading to significant variations in charging rates and ambient temperatures. This study explores the combined impact of charge rate and temperature on the degradation of lithium-ion batteries utilized in EVs, specifically focusing on lithium-ion phosphate (LFP), nickel cobalt aluminum oxide (NCA), and nickel manganese cobalt (NMC) chemistries. A novel XGBoost-Random Forest (XG-RF) model is employed for state of health (SOH) estimation, analyzing battery cycle life under varying charge rates (C/20, 1C, 2C, and 3C) and temperatures (5°C, 25°C, and 35°C) respectively. Results show that LFP batteries achieve the highest stability, with a cycle life of 5,293 cycles at 25°C and C/20, outperforming NCA and NMC. Furthermore, the proposed XG-RF model demonstrates high prediction accuracy, achieving a minimal mean squared error of 0.0006 for LFP at 25°C and C/20, but peaks at 0.4188 for NCA at 1C and 35°C, highlighting its sensitivity to extreme conditions. These findings highlight LFP's superior thermal stability and emphasize the need for optimized charging and thermal management for NCA and NMC, with the hybrid model providing accurate SOH estimation to enhance EV battery reliability and lifespan.

Keywords: battery degradation; electric vehicles; fast charging; lithium-ion batteries (LIBs); machine learning (ML); state of health (SOH)

I. INTRODUCTION

The rapid advancement of electric vehicles (EVs) necessitates significant improvements in battery technology, as the efficiency of lithium-ion batteries (LIBs) is fundamental to the widespread adoption of EVs [1–3]. Fast charging, which applies high current levels to reduce charging time, has emerged as a critical technology in EV [4,5]. However, the accelerated degradation associated with fast charging remains a major concern, as it leads to capacity fade [6,7], shorten battery lifespan [8], and increase stress [9] on internal components [10]. Additionally, the generation of excessive heat and internal pressure during fast charging heightens the risk of thermal runaway, raising serious safety concerns [11,12]. State of health (SOH) assesses battery degradation by indicating the overall status of a battery in relation to its optimal or original state [13,14]. The battery's end of life (EOL) is reached when SOH falls to 80%, indicating failure to meet the performance requirements of EVs due to reduced capacity and high safety risks [15]. Beyond this threshold, battery performance, especially during fast charging, deteriorates significantly [16]. Existing SOH estimation methods are classified as direct [17], model-based [18], and data-driven [19] machine learning (ML) models. While data-driven approaches may struggle with capturing complex relationships within the data, and model-based approaches may face challenges in accurately representing the nonlinear dynamics of LIBs, hybrid models in this case are a better approach of combination of multiple algorithms [20]. The reliability of LIBs is significantly impacted by real-world driving conditions. Prior research has revealed several operational characteristics, including charge rate [21], temperature [22], and cycling conditions [23], that affect battery health. For instance, Kumar *et al.* [24] investigated the impact of fast charging and low-temperature cycling on LIB health, revealing that low temperatures significantly increase series resistance (by 73%) and charge transfer resistance (by 16%), leading to lithium plating formation. However, this study focuses primarily on low-temperature degradation and does not comprehensively address multi-chemistry degradation trends. Han *et al.* [25] also examined thermal runaway (TR) warning signals in lithium-ion phosphate (LFP) batteries, establishing that temperature fluctuations strongly influence failure thresholds. While this study provides insights into thermal hazards, it lacks a predictive model for degradation trends across different charge rates and temperatures. Furthermore, Rahman *et al.* [26] reviewed data-driven SOH estimation techniques, emphasizing the role of AI models in battery degradation assessment. However, existing models fail to incorporate multifactor interactions explicitly, limiting real-world applicability. Qu *et al.* [27] investigated the combined effects of charge rate and operating temperature on fast-charging degradation, identifying a shift in degradation mechanisms from lithium plating at low temperatures to SEI growth at high temperatures. Nevertheless, their work is limited to single-chemistry nickel manganese cobalt (NMC) cells and lacks predictive AI-driven modeling for multi-chemistry degradation estimation at high temperature only. At high C-rates, increased LIB diffusion resistance accelerates lithium plating, leading to capacity fade and cycle life reduction [28]. Elevated temperatures further promote SEI layer growth, increasing internal resistance and irreversible lithium loss, while low temperatures exacerbate lithium plating, accelerating battery deterioration [29]. Our hybrid XGBoost-Random

Corresponding author: Namrata Mohanty (e-mail: namratamohanty@kgpian.iitkgp.ac.in).

Forest (XG-RF) model effectively captures these degradation trends, demonstrating that higher charge rates and extreme temperatures significantly accelerate SOH decline, validating the robustness of our AI-driven approach. Therefore, this study aims to address these research gaps by investigating the combined impact of charge rate and temperature on LIB degradation using a hybrid SOH estimation model. It focuses on three cell chemistries, i.e., LFP, NMC, and nickel cobalt aluminum oxide (NCA), and evaluates battery performance across four charge rates (C/20, 1C, 2C, and 3C) and three temperatures (5°C, 25°C, and 35°C). Overall, the research seeks to address the following gaps:

1. Existing studies often generalize degradation behaviors across LIB chemistries without comparing how specific operating conditions uniquely affect each chemistry.

Contribution: This paper provides a comprehensive comparison across three major LIB chemistries like LFP, NMC, and NCA, thereby highlighting the distinct degradation mechanisms under various charge rate and temperature conditions.

2. There is a lack of precise identification of optimal conditions that minimize degradation, essential for formulating safety guidelines and efficient fast charging strategies.

Contribution: This study identifies optimal charge rates and temperature ranges for each chemistry, offering actionable insights for safer and more efficient charging protocols.

3. The combined effects of high charge rates and elevated temperatures are not thoroughly quantified, particularly under realistic EV driving and charging scenarios.

Contribution: The research quantifies these combined effects, modeling how a range of charge rates and temperatures interact to impact cycle life and battery health using real-world data of EV battery degradation.

4. Current SOH estimation models frequently overlook the interactive effects of temperature and charge rate, which can be better addressed using data-driven approaches that analyze large datasets.

Contribution: The paper introduces a data-driven hybrid SOH estimation model that leverages extensive datasets to capture these interactive effects, enhancing the accuracy and reliability of battery health predictions.

By understanding these effects, charging protocols can be tailored to minimize degradation, ensuring more efficient energy usage and cost-effectiveness in EV operations. The subsequent sections of this work are organized as follows: Section II introduces the model framework for SOH estimation. Section III describes the joint impact of parameters on battery health, succeeded by results and observations in Section IV. The conclusions are summarized in Section V, accompanied by relevant references.

II. MODEL STRUCTURE AND ALGORITHM

This paper utilizes a dataset on INR21700-M50T LIB cells tested at the Stanford Energy Control Laboratory over a 23-month period, following the urban dynamometer driving schedule (UDDS) [30]. Designed to simulate real-world driving conditions, the UDDS protocol includes various speeds and accelerations, making it particularly suitable for assessing EV batteries. Tests were conducted across multiple charge rates and temperature ranges, exploring how these factors influence battery performance and degradation. The UDDS dataset is utilized in this study is not for direct electrochemical analysis but as a real-world dataset to train and validate the data-driven model. Here the model learns from historical battery performance data, identifying SOH trends under varying charge rates and temperature conditions rather than explicitly modeling degradation mechanisms. This study presents a hybrid XGBoost-random forest (XG-RF) model for SOH estimation in LIBs addressing degradation influenced by charging rate and temperature variations. The methodology details model construction, parameter selection, data preprocessing, training strategies, input variables, target variables, and model architecture to ensure a robust and scalable approach to battery health prediction. In this hybrid model, XGBoost (XG) and random forest (RF) are integrated to capitalize on their unique strengths in pattern recognition and ensemble learning. XG is highly efficient in handling structured data, offering speed and precision, while RF prevents overfitting by averaging multiple decision trees. Together, the XG-RF model enhances predictive accuracy, providing a more nuanced understanding of complex interactions between operational factors affecting battery health. The model utilizes battery voltage, current, and surface temperature as key input parameters, selected due to their strong correlation with capacity fade and thermal stress, both of which directly impact battery degradation. This hybrid framework effectively captures degradation patterns and predicts SOH across diverse operational conditions, crucial for real-world EV applications where frequent fast charging and fluctuating environmental factors influence battery longevity. To optimize model performance, a grid search-based hyperparameter tuning strategy was employed, refining learning rate, max depth, number of estimators, gamma, and min samples split for both models. The data preprocessing pipeline includes outlier detection using z-score thresholding and interquartile range filtering, feature extraction based on XGBoost gain values, and dimensionality reduction via principal component analysis to optimize computational efficiency. A fivefold cross-validation training strategy with an 80–20 train-test split was implemented to enhance generalization. The model architecture consists of three stages: (1) Feature selection using XG to rank the most critical variables for degradation modeling, (2) boosting and training, where XG iteratively reduces prediction errors by adjusting feature weights, and (3) final prediction refinement using RF for ensemble averaging and improved SOH estimation accuracy, i.e., a critical metric that quantifies battery health, obtained by accessing the actual capacity divided by nominal capacity as shown in the following equation (1), where, Q_{act}, Q_{nom} represent the actual capacity and nominal capacity respectively [31]. Flowchart of the SOH estimation method is explained in Fig. 1 stepwise.

$$SOH = \frac{Q_{act}}{Q_{nom}} \tag{1}$$

A. FEATURE SELECTION

Feature selection is a crucial step in ML models, particularly SOH estimation, as irrelevant or redundant features can

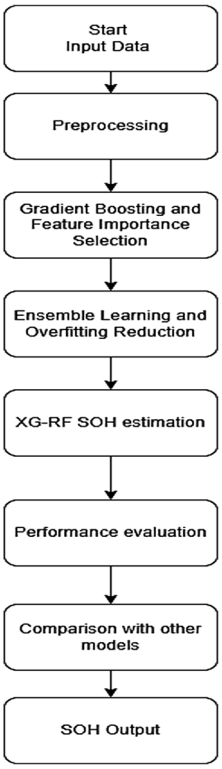

Fig. 1. Flowchart of SOH estimation method for LIBs.

negatively impact model performance. XG is used in this study for feature selection due to its ability to assign importance scores to different input variables, allowing us to rank features based on their contribution to predicting SOH. XG assigns an importance score (I_f) to each feature (f) based on the gain it provides in reducing prediction error across all decision trees as in equation (2).

$$I_f = \sum_{t=1}^{T} G_t(f) \tag{2}$$

where, G_t represents the gain from splitting on feature f in tree t and T is the total number of trees in the model. A higher importance score indicates here that current, voltage, and surface temperature have a stronger influence on battery SOH estimation, whereas other recorded low importance scores are removed to improve efficiency and reduce model complexity.

B. BOOSTING AND TRAINING

Gradient boosting is an iterative learning process where new model learns from the previous errors of previous models, improving accuracy over time. In this paper, XG builds a sequence of decision trees, each reducing the residual errors of its predecessor. The boosting process is represented as equation (3).

$$F_m(x) = F_{m-1}(x) + \gamma h_m(x) \tag{3}$$

where $F_m(x)$ is the model at iteration m, $F_{m-1}(x)$ is the previous model iteration, $h_m(x)$ is the new decision tree added at iteration, m and γ are the learning rates, controlling the contribution of $h_m(x)$. XG optimizes its model by minimizing a loss function L, which consists of $\sum_{i=1}^{N} l(y_i \widehat{\hat{y}i})$ as loss function, measuring the difference between actual and predicted SOH, and $\lambda \sum_{j=1}^{T} \|w_j\|^2$ as regularization term, showing penalizing model complexity to prevent overfitting as in equation (4).

$$L = \sum_{i=1}^{N} l(y_i \widehat{\hat{y}i}) + \lambda \sum_{j=1}^{T} \|w_j\|^2 \tag{4}$$

C. PREDICTION REFINEMENT AND ENSEMBLE AVERAGING

The final stage of the hybrid model involves RF, which refines SOH estimation using ensemble averaging. The final SOH estimate is computated as equation (5).

$$\hat{y} = \frac{1}{T} \sum_{t=1}^{T} f_t(x) \tag{5}$$

with $\hat{y}$ as final predicted SOH, $f_t(x)$ as prediction from decision tree t, and T as total number of trees in the model. This ensemble learning approach reduces variance, making SOH estimation more stable and robust.

III. PARAMETER EFFECT ON BATTERY HEALTH

This section examines the performance of various battery chemistries at different charge rates (C/20, 1C, 2C, and 3C) at distinct temperatures (5°C, 25°C, and 35°C), respectively.

Our study employs an ML-based SOH estimation approach rather than a physics-based electrochemical model, allowing for data-driven insights into battery degradation trends without requiring predefined electrochemical equations. Unlike traditional model-based methods, which rely on fixed mathematical assumptions and struggle with real-world variability, ML dynamically adapts to different charge rates, temperatures, and chemistries, ensuring higher accuracy and generalization. The correlation between battery performance and the number of charge or discharge cycles under diverse settings can be depicted by SOH vs cycle curve. An in-depth analysis of the interaction among these variables is crucial for formulating effective solutions to reduce degradation and extend the lifespan of LIBs, facilitating a better understanding of optimal charging strategies. This parameter effect on the battery degradation analysis is discussed in subsequent subsections. To improve model robustness, we incorporated multiple datasets, ensuring the model's ability to generalize across different battery chemistries, operating conditions, and environmental stress factors.

A. LFP BATTERIES

For LFP batteries, Fig. 2 illustrates the SOH versus cycle curve across different charge rates and temperatures. At 5°C, the cycle life reaches 5075 cycles at a C/20 charge rate, highlighting minimal degradation due to reduced lithium plating and lower stress on the cell components. However, as the charge rate increases to 1C, the cycle life decreases markedly to 4021 cycles, primarily attributed to heightened internal resistance and intensified lithium plating effects. At a 2C charge rate, the cycle life declines further to 2940 cycles, underscoring the cumulative impact of accelerated

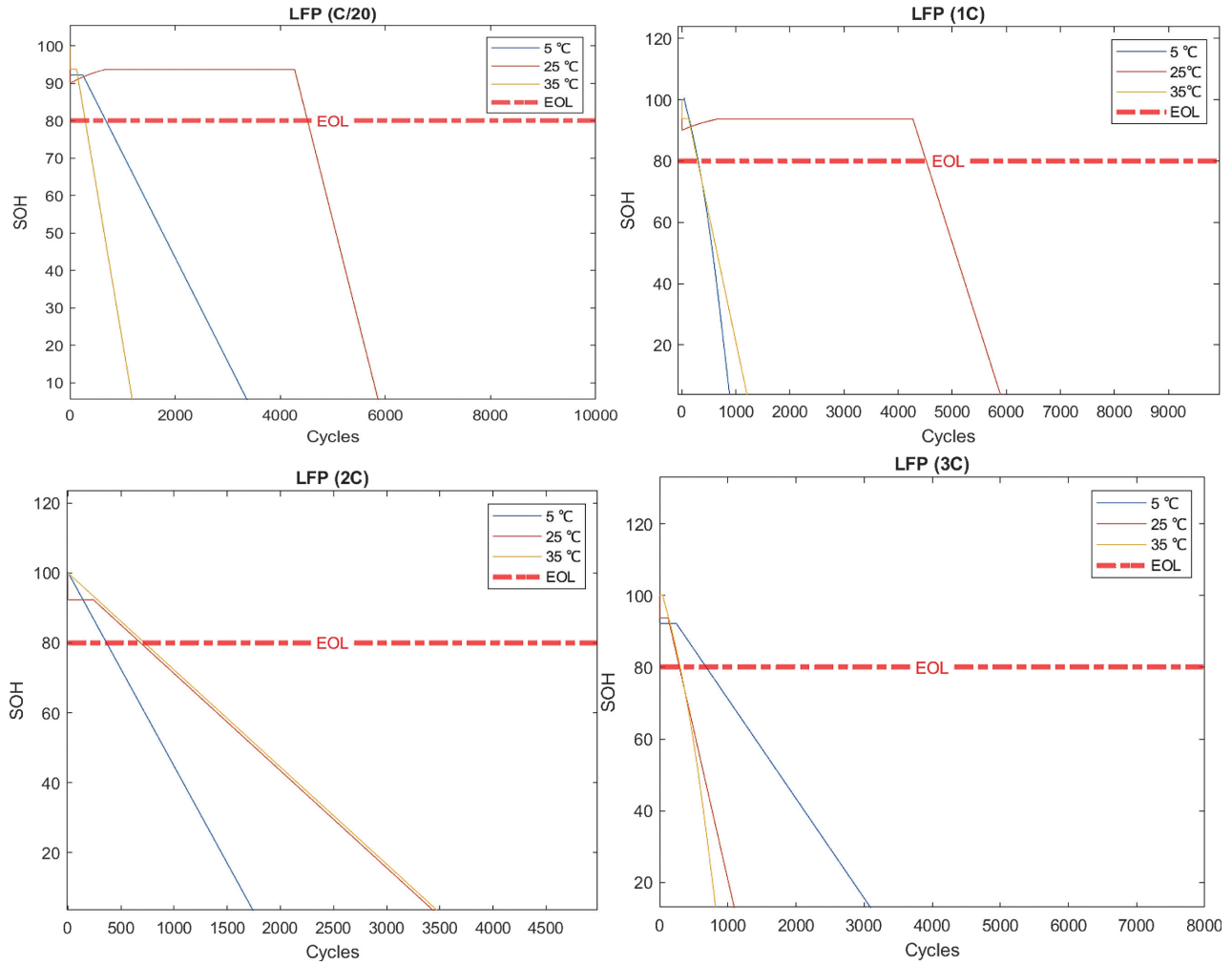

Fig. 2. SOH vs cycle curve for LFP batteries for different temperatures at different charge rates: C/20, C, 2C, and 3C.

Table I. Results for obtained cycle life for LFP batteries

	Cycle life (EOL of first life)		
Charge rates	**5°C**	**25°C**	**35°C**
C/20	5075	6156	4579
1C	4021	5383	3500
2C	2940	3579	2296
3C	1396	1550	1034

degradation mechanisms. At the highest charge rate of 3C, the cycle life plummets to 1396 cycles, reflecting the adverse effects of increased stress on chemical stability. A similar trend is observed at 35°C, where the cycle life significantly decreases from 4579 cycles at a C/20 charge rate to 1034 cycles at 3C. The pronounced reduction in cycle life at higher charge rates and elevated temperatures is indicative of exacerbated degradation mechanisms, including increased electrolyte decomposition and lithium plating.

Table I presents the obtained cycle life results for LFP batteries, where cycle life decreases sharply with higher charge rates, highlighting the sensitivity of LFP batteries to extreme temperature and charge rate.

B. NCA BATTERIES

For NCA batteries, from Fig. 3, it has been observed that the cycle life exhibits a notable response to varying charge rates and temperatures. At a 5°C temperature, the cycle life at a C/20 charge rate is relatively low, recording only 1,392 cycles. This observation underscores the high sensitivity of NCA chemistry to temperature extremes, even at slower charge rates. Increasing the charge rate to 1C results in an improvement in cycle life to 1,083 cycles, suggesting that the enhanced ion mobility at this rate partially mitigates the adverse effects of the cooler temperature. However, further increases in the charge rate to 2C and 3C lead to a marked decline in cycle life, with values dropping to 671 cycles and 564 cycles, respectively. This reduction can be attributed to accelerated thermal and electrochemical degradation processes, highlighting the importance of managing charge rates and temperature to optimize the performance and longevity of NCA batteries.

Table II presents the obtained cycle life results for NCA batteries, where the batteries exhibit greater sensitivity to both low and high temperatures, with a sharper decline in cycle life at extreme charge rates, whereas LFP batteries generally show more stable performance across a wider temperature range.

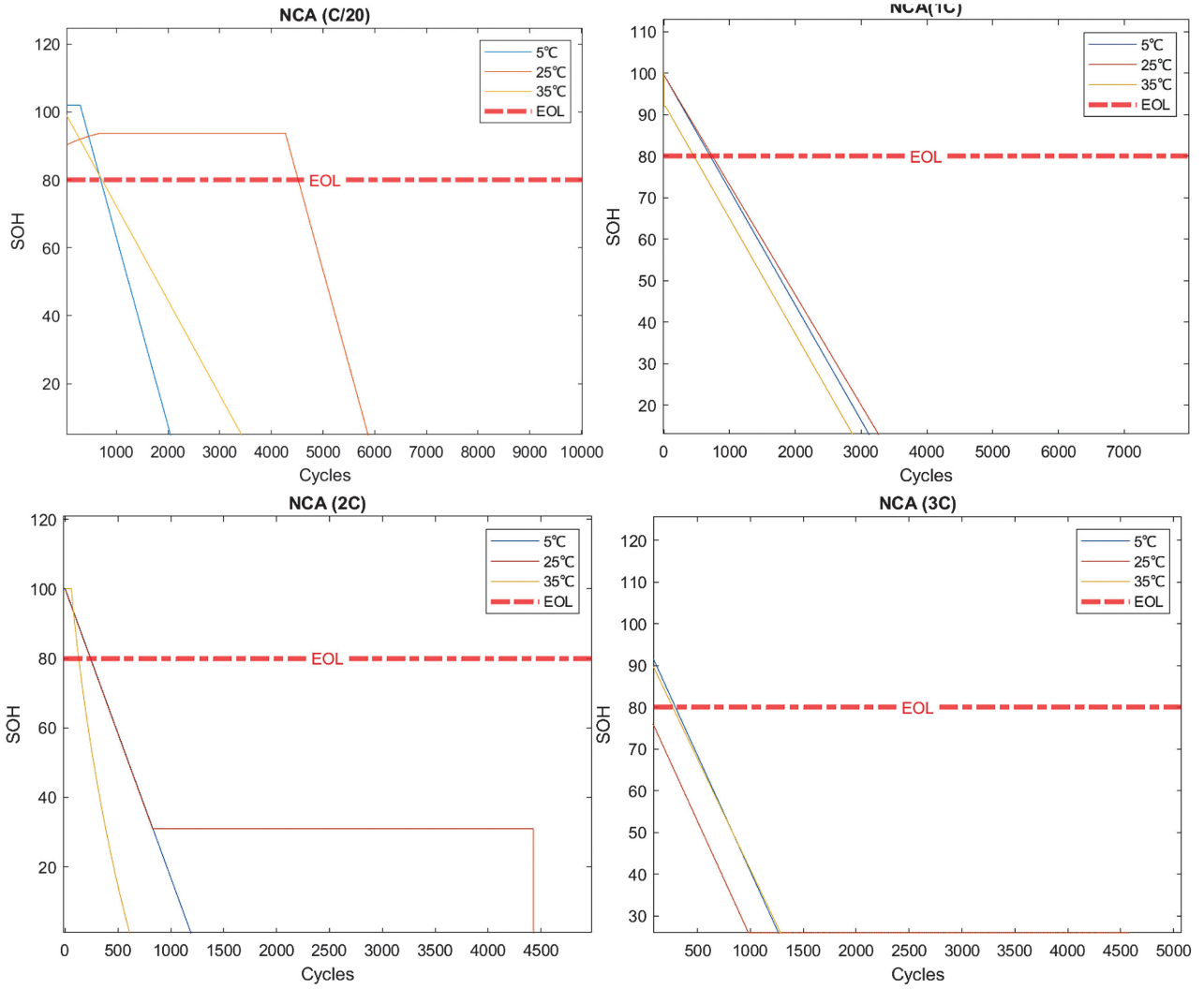

Fig. 3. SOH vs cycle curve for NCA batteries for different temperatures at different charge rates: C/20, C, 2C, and 3C.

Table II. Results for obtained cycle life for NCA batteries

	Cycle life (EOL of first life)		
Charge rates	**5°C**	**25°C**	**35°C**
C/20	1392	4802	1409
1C	1083	1294	951
2C	671	693	369
3C	564	500	532

C. NMC BATTERIES

Similarly, for NMC batteries, from Fig. 4, at 5°C, the cycle life is observed to be 477 cycles at a C/20 charge rate, indicating a balanced performance under cooler conditions. However, increasing the charge rate to 1C results in a decline to 648 cycles, where degradation effects begin to manifest more significantly. At a charge rate of 2C, the cycle life decreases further to 340 cycles, and at 3C, it drops to only 139 cycles, illustrating the limitations of this chemistry under high charge rates. At 25°C, NMC batteries achieve a cycle life of 951 cycles at a C/20 charge rate, benefiting from optimal thermal conditions that reduce internal resistance and enhance overall performance. Yet, as the temperature rises to 35°C, the cycle life is still impacted negatively, yielding 876 cycles at C/20. This pattern highlights the detrimental effects of elevated temperatures on cycle life, especially when combined with higher charge rates, where the performance becomes notably compromised, yielding only 646 cycles at a 3C rate. The data clearly demonstrates the sensitive balance between charge rates and temperatures in maintaining the long-term stability of NMC batteries.

Table III presents the obtained cycle life results for NCA batteries that demonstrate the most consistent performance, especially at low temperatures. Compared to LFP and NCA, NMC batteries show more variability in performance across different temperatures, with better stability, but a rapid decline at both low and high temperatures.

These plots highlight distinct degradation patterns, emphasizing the impact of charging conditions on the longevity and reliability of each battery chemistry.

IV. RESULTS AND DISCUSSION

In this section, through 3D surface plots, contour plots, and interaction plots, we explore resilience, operational limits,

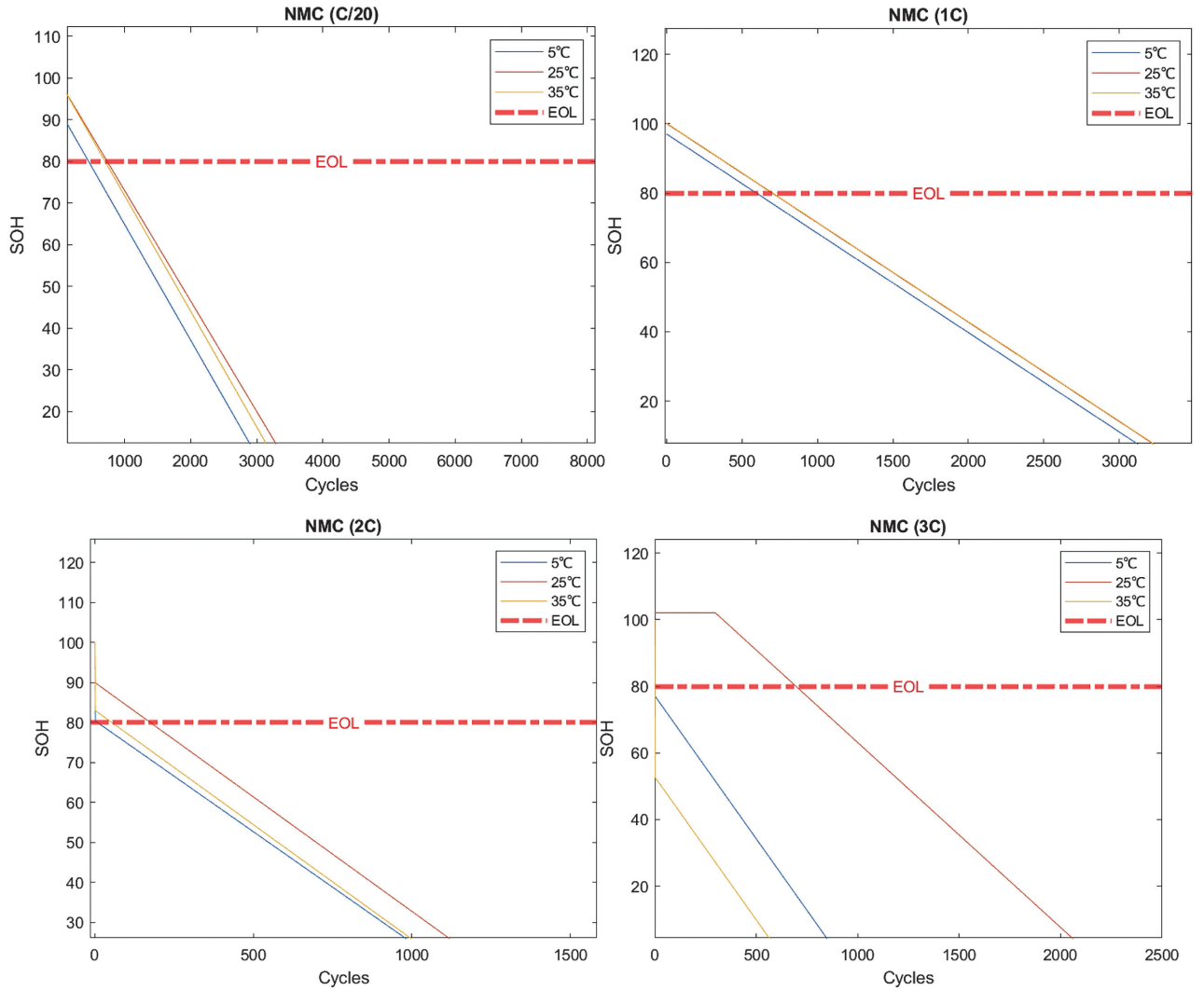

Fig. 4. SOH vs cycle curve for NMC batteries for different temperatures at different charge rates: C/20, C, 2C, and 3C.

Table III. Results for obtained cycle life for NMC batteries

	Cycle life (EOL of first life)		
Charge rates	**5°C**	**25°C**	**35°C**
C/20	477	951	876
1C	648	821	809
2C	340	732	320
3C	139	646	94

and optimal usage conditions of each type of battery for effective battery management strategies.

A. 3D SURFACE AND CONTOUR PLOTS

This section analyses the 3D surface and contour plots for each battery chemistry, illustrating the impact of charge rate and temperature on cycle life. It highlights optimal zones and performance boundaries, particularly emphasizing how each battery chemistry tolerates various conditions. The discussion compares the gradual versus steep declines in cycle life across LFP, NCA, and NMC batteries, providing insights into their resilience and degradation rates under different conditions.

For LFP batteries, the 3D surface plot shown in Fig. 5 exhibits a relatively smooth topology with a broad range of high cycle counts at lower charge rates of C/20 and moderate temperatures of 25°C. This indicates that LFP batteries perform optimally under these conditions, demonstrating less sensitivity to temperature variations compared to other chemistries.

The contour plot shown in Fig. 6 further reinforces this observation by showing a concentrated region of high cycle life around the C/20 charge rate and 25°C, suggesting that these parameters minimize degradation effects. However, as the charge rate increases and temperatures reach extreme levels of 5°C and 35°C, the cycle life declines sharply, highlighting the limitations of LFP batteries under stressful conditions. This decline is attributed to factors such as increased internal resistance and enhanced lithium plating at higher charge rates and temperatures, which accelerate degradation mechanisms.

The 3D surface plot for NCA batteries illustrated in Fig. 7 displays steeper slopes, particularly at elevated temperatures, indicating a higher sensitivity to both charge rate and temperature changes. As the charge rate increases,

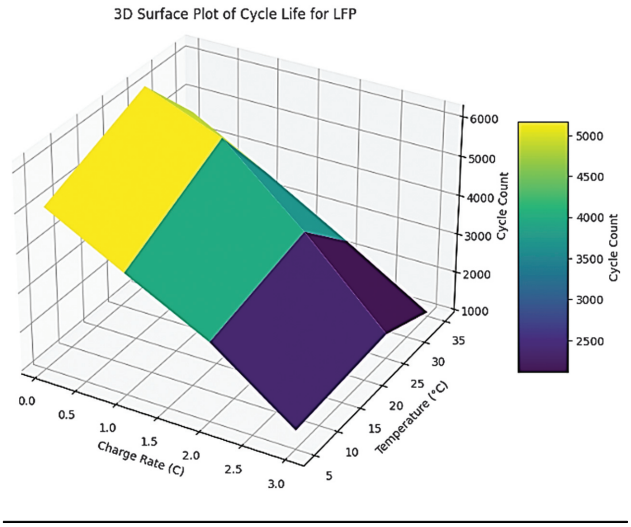

Fig. 5. 3D surface plot of cycle life for LFP.

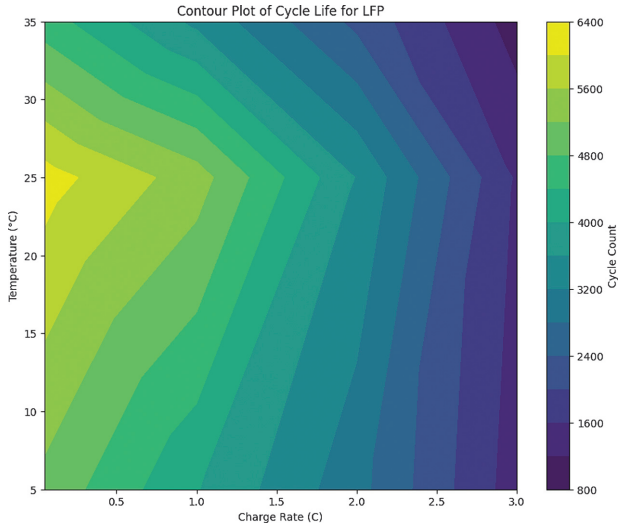

Fig. 6. Contour plot of cycle life for LFP.

there is a noticeable decline in cycle life at higher temperatures, reflecting the rapid degradation of battery performance under stressful conditions.

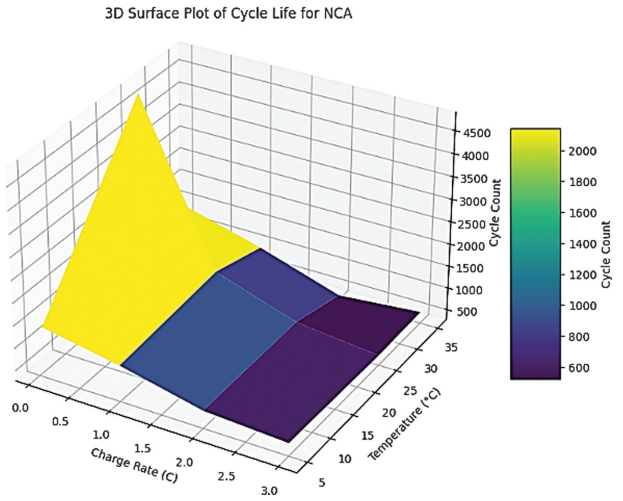

Fig. 7. 3D surface plot of cycle life.

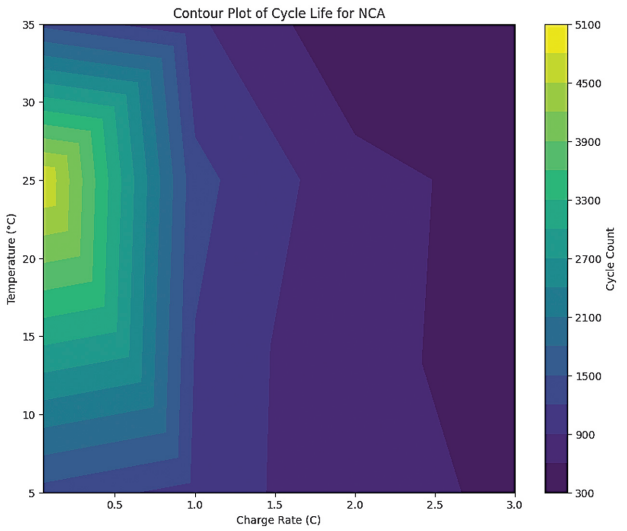

Fig. 8. Contour plot of cycle life for NCA.

The contour plot for NCA batteries is displayed in Fig. 8 reveals a rapid drop in cycle life as both charge rate and temperature increase, with dense contour lines at higher charge rates and temperatures illustrating the steep performance degradation. This steep decline underscores the pronounced sensitivity of NCA batteries to thermal stress and fast charging, necessitating stringent thermal management and controlled charging protocols to maintain battery longevity.

NMC batteries exhibit a more balanced performance across varying charge rates and temperatures, as depicted in the 3D surface plot in Fig. 9. While the cycle life remains relatively high at moderate charge rates and temperatures, there is a noticeable decline at both low 5°C and high 35°C temperatures, especially under high charge rates of 3C. The contour plot for NMC in Fig. 10 displays a mixed response similar to NCA, with a gradual drop in cycle life at higher charge rates and temperatures. However, the contours are not as sharply defined as those for NCA, suggesting that NMC chemistry tolerates higher charge rates and temperatures slightly better than NCA. The areas of optimal performance are still concentrated around lower charge rates

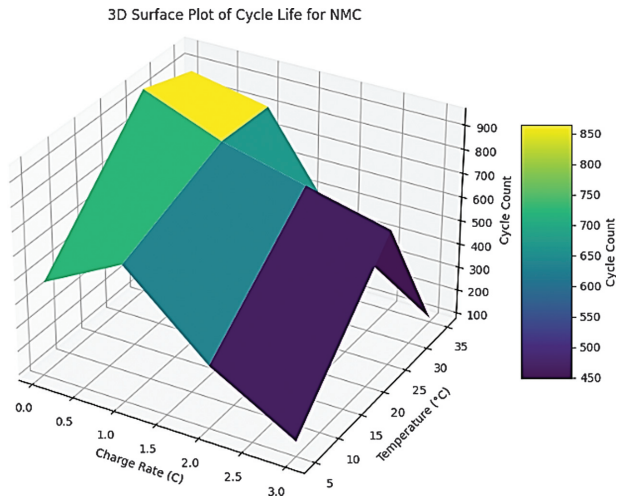

Fig. 9. 3D surface plot of cycle life for NMC.

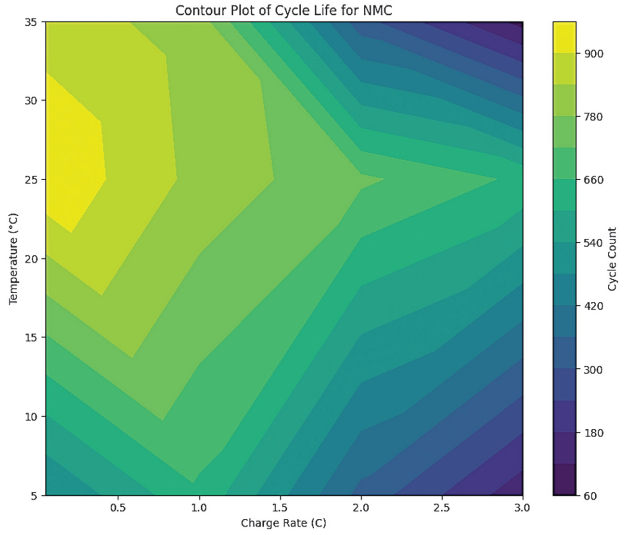

Fig. 10. Contour plot of cycle life for NMC.

and moderate temperatures, although the degradation is less severe compared to NCA.

Comparing the three chemistries, LFP batteries demonstrate the greatest resilience to varying charge rates and temperatures, maintaining high cycle life under moderate conditions. NMC batteries offer a balanced performance with moderate sensitivity, while NCA batteries are the most susceptible to degradation under extreme charge rates and temperatures. These insights from the 3D surface and contour plots emphasize the necessity for tailored charging and thermal management strategies for each battery chemistry to optimize performance and extend battery lifespan in EV applications.

B. INTERACTION PLOT

The interaction plot for LFP batteries shown in Fig. 11 highlights the combined effects of charge rate and temperature on cycle life. At lower charge rates, such as C/20, the cycle life remains consistently high across all temperature conditions, demonstrating the robustness of LFP chemistry under low-stress operational conditions. However, as the charge rate increases to 1C, 2C, and 3C, a significant decline in cycle life is observed, particularly at elevated temperatures. At 35°C, the degradation becomes more

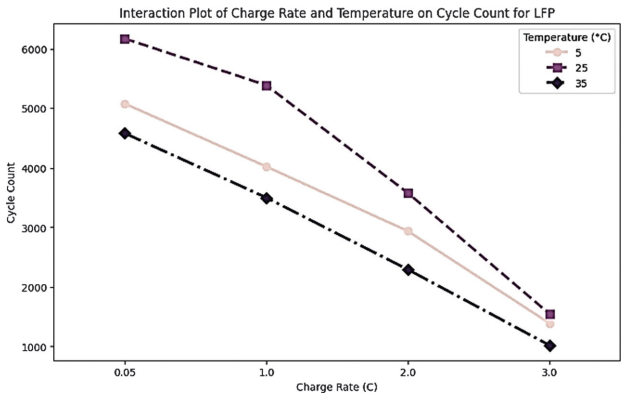

Fig. 11. Interaction plot of charge rate and temperature on cycle count for LFP.

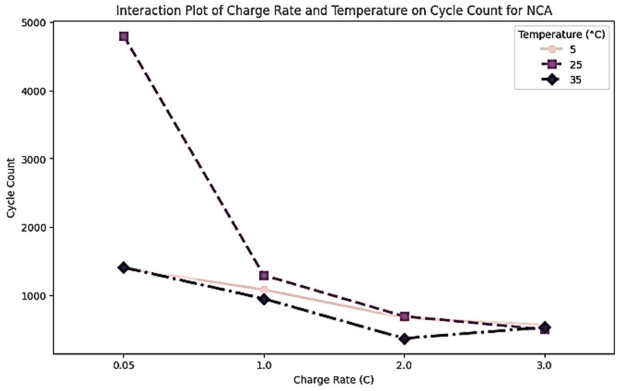

Fig. 12. Interaction plot of charge rate and temperature on cycle count for NCA.

pronounced, reflecting the compounding effects of high charge rates and thermal stress on the battery's chemical stability and internal structure. This suggests that while LFP batteries are well-suited for applications requiring moderate charge rates and temperatures, their performance diminishes when subjected to aggressive charging and heat. The plot underscores the importance of maintaining optimal operational conditions to prolong cycle life, particularly for high-demand applications. Overall, LFP batteries exhibit strong performance at low charge rates across varying temperatures but face accelerated degradation as charge rates and thermal stress increase.

The interaction plot for NCA chemistry shown in Fig. 12 shows a significant sensitivity to changes in both charge rate and temperature. Cycle life decreases steeply as either the charge rate or temperature increases. The most drastic reductions are observed at higher charge rates (2C and 3C) and higher temperatures (35°C), indicating that NCA batteries are highly susceptible to degradation under these stressful conditions. The interaction emphasizes the importance of maintaining lower temperatures and slower charge rates to maximize NCA battery longevity.

The interaction plot for NCA chemistry shown in Fig. 12 shows a significant sensitivity to changes in both charge rate and temperature. Cycle life decreases steeply as either the charge rate or temperature increases. The most drastic reductions are observed at higher charge rates (2C and 3C) and higher temperatures (35°C), indicating that NCA batteries are highly susceptible to degradation under these stressful conditions. The interaction emphasizes the importance of maintaining lower temperatures and slower charge rates to maximize NCA battery longevity.

Similarly, the interaction plot for NMC chemistry shown in Fig. 13 highlights a more balanced performance compared to NCA, but with a clear decline in cycle life as the charge rate and temperature increase. At a moderate temperature of 25°C and lower charge rates, NMC batteries sustain a relatively high cycle life. However, similar to NCA, the combination of high charge rates and high temperatures (such as 3C and 35°C) significantly shortens the cycle life. This observation suggests that while NMC batteries can tolerate moderate stress, extreme conditions accelerate their aging process.

The cycle life for LFP batteries is highest at lower charge rates, especially at C/20. It significantly decreases as the charge rate increases to 2C and 3C, indicating that LFP

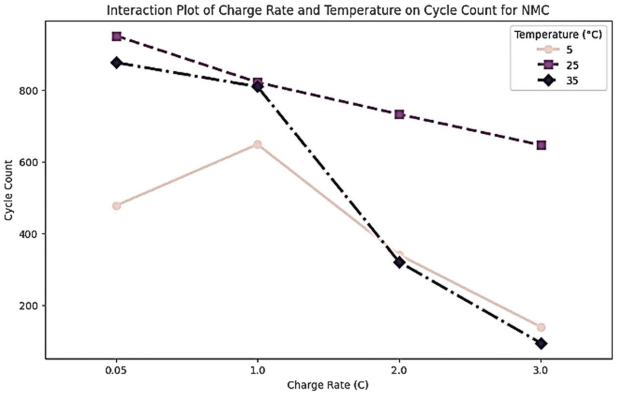

Fig. 13. Interaction plot of charge rate and temperature on cycle count for NMC.

batteries can withstand slow charging well but degrade faster under high charge rates. Temperature also plays a crucial role as at lower temperatures like 5°C and 25°C, LFP batteries show better cycle life compared to 35°C. However, the decrease in cycle life due to temperature is less drastic than for NCA or NMC chemistries, showcasing LFP's relatively higher tolerance to thermal stress.

In addition to the primary dataset, another dataset was considered for this study, consisting of 28 lithium-ion cells tested under controlled conditions to analyze SOH degradation trend [32]. This dataset includes four temperature levels (0°C, 10°C, 25°C, and 45°C) and two charge rates (0.5C and 1C), allowing for a comprehensive evaluation of charge rate–temperature interactions on battery health. The sensitivity analysis using the XG-RF model reveals that charge rate and temperature significantly influence SOH degradation trends in LIBs. Fast charging (1C) accelerates SOH decline, particularly at extreme temperatures (0°C and 45°C), where lithium plating and SEI layer growth dominate degradation mechanisms. In contrast, moderate charge rates (0.5C) at optimal temperatures (25°C–35°C) maintain higher SOH over extended cycles, confirming that lower charging stress improves battery longevity. Feature

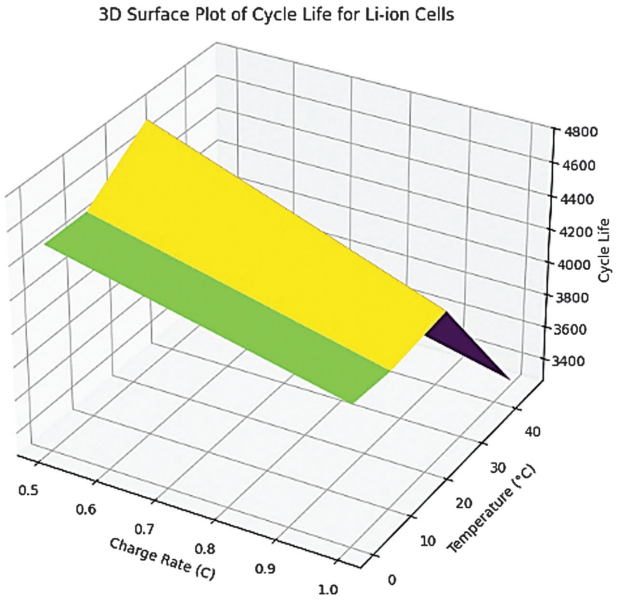

Fig. 14. 3D surface plot of cycle life.

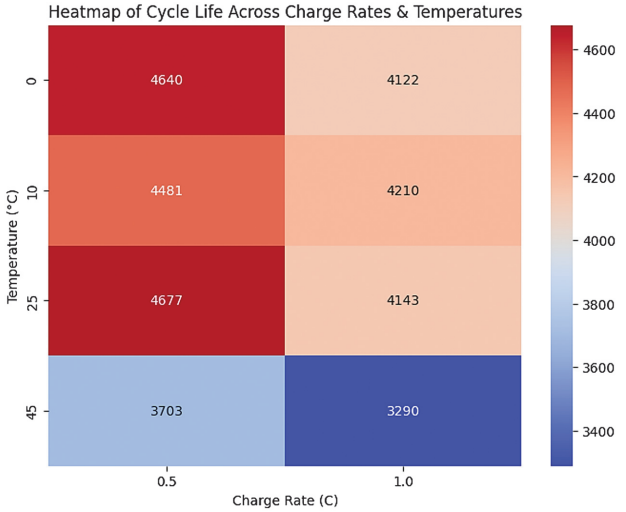

Fig. 15. Heatmap of cycle life across charge rates and temperatures.

importance analysis from the XG-RF model indicates that charge rate has a stronger impact on SOH than temperature variations, as higher C-rates induce greater electrochemical stress. The 3D surface plot of SOH vs. cycle life shown in Fig. 14 illustrates a nonlinear degradation pattern, emphasizing the complex interactions between charge rate and thermal conditions. Heatmap analysis shown in Fig. 15 with interaction plot shown in Fig. 16 further confirms that optimal SOH retention occurs at 0.5C and moderate temperatures, while rapid degradation is observed at 1C and extreme temperature ranges. These findings validate that the hybrid XG-RF model effectively captures charge rate-temperature dependencies in SOH estimation, making it a robust tool for real-world EV battery health prediction and degradation analysis.

The proposed XG-RF SOH estimation model was applied to LFP, NMC, and NCA battery chemistries, revealing distinct degradation trends influenced by charge rate and temperature. LFP demonstrated stability at moderate charge rates (C/20 – 1C) but degraded rapidly under fast charging (>2C) at extreme temperatures (<10°C or >45°C). NMC exhibited faster degradation at elevated temperatures (>40°C) due to SEI layer growth, while NCA showed accelerated SOH decline at high charge rates (>2C) above 35°C, aligning with known cathode instability

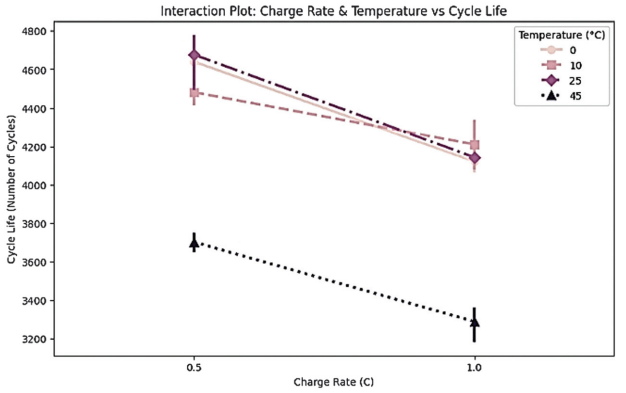

Fig. 16. Interaction plot of cycle life across charge rates and temperatures.

issues. The degradation patterns observed across different chemistries confirm the reliability of our AI-based SOH estimation model. The results indicate that LFP batteries are most affected by low-temperature lithium plating, while NMC and NCA chemistries experience capacity loss primarily due to SEI growth and cathode breakdown at high temperatures. These findings validate that ML-based SOH estimation can effectively capture chemistry-specific degradation behaviors, reinforcing its applicability across diverse battery types and operational conditions. By integrating charge rate–temperature interactions with chemistry-specific degradation analysis, our study demonstrates that proposed SOH estimation framework can provide accurate and adaptable predictions for real-world EV applications. Future work could incorporate additional chemistries and real-time operational datasets to further refine SOH estimation accuracy.

While vehicle load dynamics and speed variations contribute to battery degradation, this study isolates charge rate and temperature as the primary influencing factors. Future research could integrate driving load variations to enhance SOH prediction under real-world EV operating conditions

C. PERFORMANCE EVALUATION

The performance evaluation and model validation are facilitated by the actual vs. predicted SOH plots and error plots, which are displayed in Figs. 17 and 18, respectively, and provide a visual assessment of the model's efficacy. The purpose of the actual vs. predicted SOH plot is to give an intuitive visual representation of how well the model captures the complex dynamics of battery degradation. SOH error plots also provide information about areas with high predictive accuracy and those that need more work. Performance of proposed model in predicting the SOH of LIBs, in terms of mean squared error (MSE) values demonstrate considerable variation across different chemistries (LFP, NCA, and NMC) under diverse charge rates and temperatures, is shown in Tables IV–VI.

For LFP batteries, the model achieves high accuracy at moderate temperature, i.e., 25°C and high, i.e., 35°C temperatures, particularly at a slow charge rate of C/20, where the lowest MSE of 0.0006 is recorded. However, at low temperatures of 0°C, the model's accuracy declines, evident from a higher MSE of 0.0312 at C/20, indicating reduced predictive reliability in cold conditions. In contrast, NCA batteries display the most inconsistency, especially at extreme temperatures. The MSE peaks at 0.2235 for a 2C rate at 0°C and reaches 0.4188 at 35°C under a 1C charge rate, revealing a heightened sensitivity of NCA batteries to temperature extremes, particularly under fast charging. Nonetheless, the model shows improved accuracy for NCA at 25°C, with a minimal MSE of 0.0019 at 1C.

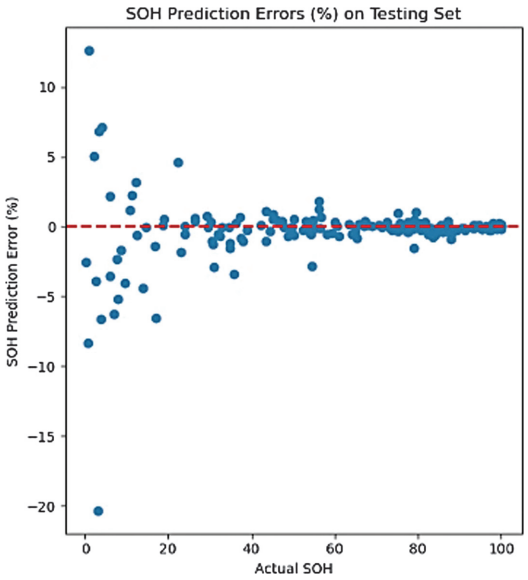

Fig. 18. Prediction error plot.

Table IV. MSE values for XG-RF model for different charge rates and temperatures for LFP batteries

	0°C	25°C	35°C
C/20	0.0312	0.0013	0.0006
1C	0.0015	0.0018	0.0013
2C	0.0020	0.0025	0.0023
3C	0.0027	0.0018	0.0023

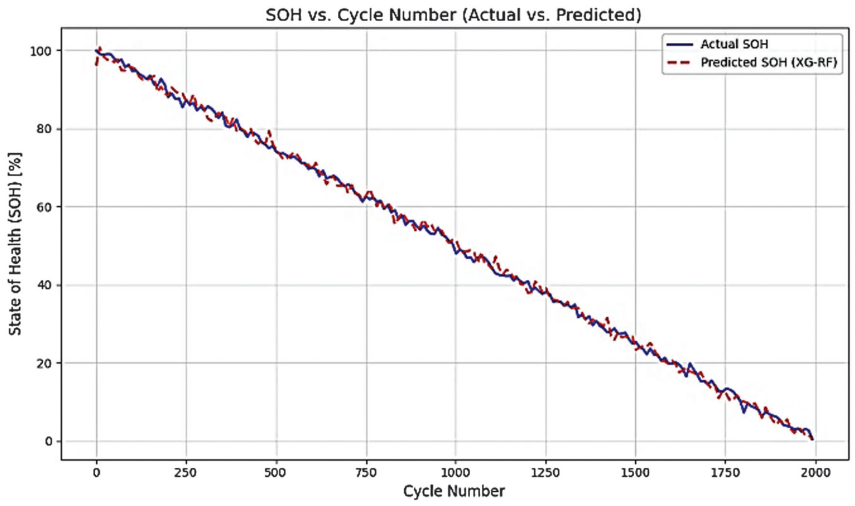

Fig. 17. Actual vs predicted SOH with XG-RF.

Table V. MSE values for XG-RF model for different charge rates and temperatures for NCA batteries

	0°C	25°C	35°C
C/20	0.0125	0.4677	0.1171
1C	0.0553	0.0019	0.4188
2C	0.2235	0.0449	0.2352
3C	0.0125	0.0964	0.0106

Table VI. MSE values for XG-RF model for different charge rates and temperatures for NMC batteries

	0°C	25°C	35°C
C/20	0.2299	0.0100	0.0103
1C	0.1050	0.0090	0.1017
2C	0.0054	0.0105	0.0085
3C	0.0086	0.0090	0.0106

NMC batteries exhibit relatively stable performance across all temperatures and charge rates, though higher errors are observed at low temperatures, notably an MSE of 0.2299 at C/20. Consistency improves at moderate temperatures (25°C), yielding low MSE values across various charge rates.

Overall, the model achieves optimal predictive accuracy for LFP and NMC batteries at 25°C but encounters challenges with NCA batteries under extreme conditions. The MSE values underscore the importance of moderate temperature ranges for reliable SOH predictions, while the pronounced variability in NCA performance highlights a significant sensitivity to temperature and charge rate fluctuations. These findings underscore the critical need for precise thermal and charge management to optimize battery health monitoring and enhance SOH estimation reliability across different chemistries. Further research is warranted to delve into the factors influencing battery degradation and to refine model accuracy under varying operating conditions, supporting more effective predictive maintenance in EV applications.

The comparative analysis of SOH estimation models was conducted using multiple ML approaches, including proposed XG-RF, SVM, LSTM, XGBoost, AdaBoost, decision tree, gradient boosting (GBM), and KNN. The results, summarized in Table VII, indicate that XG-RF achieved the highest accuracy, with the lowest MAE (0.012) and highest R^2 score (0.998), confirming its effectiveness in predicting battery SOH over cycle life. The LSTM model also demonstrated strong performance (MAE: 0.015, R^2: 0.996), benefiting from its sequential learning capability, while GBM and XGBoost exhibited comparable accuracy levels (R^2: 0.996 and 0.995, respectively). In contrast, traditional models such as decision tree and KNN showed relatively lower accuracy, with MAE values exceeding 0.025.

Figure 19 illustrates the SOH vs. cycle life curves for different ML models, highlighting the superior predictive accuracy of XG-RF, which closely follows actual SOH trends. Models such as LSTM and gradient boosting also exhibit strong performance, while traditional models like decision tree and KNN show greater deviations from actual SOH values. The SOH vs. cycle life curves further highlight

Table VII. Performance evaluation of proposed model comparison across different models

Model	MAE	R^2
XG-RF	0.003335	0.999774
SVM	0.022341	0.987187
LSTM	0.052470	0.935914
XGBoost	0.003046	0.999806
AdaBoost	0.018907	0.993418
Decision tree	0.006053	0.999294
Gradient boosting	0.003930	0.999676
KNN	0.006425	0.999102

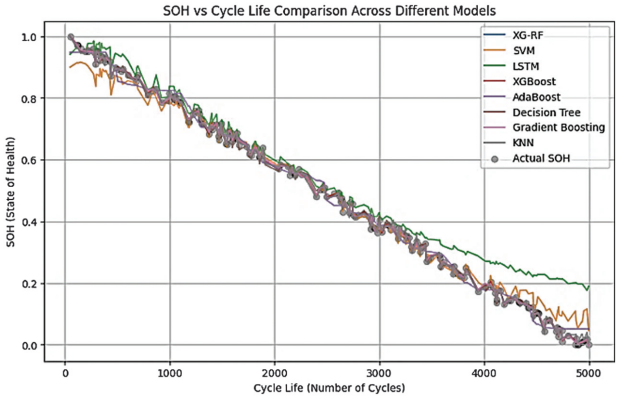

Fig. 19. SOH vs cycle life comparison across different models.

the capability of ensemble learning models, particularly XG-RF, in capturing the nonlinear degradation trends of LIBs across different operating conditions.

This analysis validates the importance of hybrid ensemble techniques for robust SOH estimation, demonstrating their applicability in real-world EV battery health monitoring and predictive maintenance strategies.

The next section will discuss the necessity for deeper insights into battery behavior under diverse thermal and charging environments. The results underscore the varied performance attributes of these three battery chemistries at different charge rates and temperatures. This highlights the necessity of optimizing thermal management and charging procedures for batteries to improve the overall performance and longevity of various battery chemistries in EVs.

V. CONCLUSION

This study explored the combined effects of charge rate and temperature on the degradation of LIBs in EVs focusing on LFP, NCA, and NMC chemistries. Using a hybrid XG-RF, the analysis revealed that LFP batteries demonstrate the highest stability, achieving 5,293 cycles at 25°C and C/20, making them suitable for applications requiring long lifespan and safety. NCA batteries, while offering high energy density, degrade rapidly under extreme conditions, with cycle life reducing to 500 cycles at 35°C and 3C. NMC batteries exhibited moderate performance but were particularly vulnerable to fast charging and elevated temperatures, with cycle life dropping to 94 cycles under the same conditions. Proposed XG-RF model provided accurate SOH estimations, achieving an MSE as low as 0.0006

for LFP at optimal conditions, although it showed reduced accuracy for NCA under extreme environments, with an MSE of 0.4188 at 35°C and 1C. These results highlight the superior thermal stability of LFP batteries and the critical need for optimized charging protocols and thermal management strategies for NCA and NMC chemistries to mitigate degradation and ensure reliability. Future research should focus on refining charging strategies, enhancing thermal management techniques, and exploring advanced chemistries to improve the durability and efficiency of LIBs in real-world EV applications.

CONFLICT OF INTEREST STATEMENT

The authors declare no conflicts of interest.

REFERENCES

[1] T. R. Tanim et al., "A comprehensive understanding of the aging effects of extreme fast charging on high Ni NMC cathode," *Adv. Energy Mater.*, vol. 12, no. 22, pp. 1–17, 2022.

[2] P. K. Tarei, P. Chand, and H. Gupta, "Barriers to the adoption of electric vehicles: evidence from India," *J. Clean. Prod.*, vol. 291, p. 125847, 2021.

[3] M. A. Hannan, M. S. H. Lipu, A. Hussain, and A. Mohamed, "A review of lithium-ion battery state of charge estimation and management system in electric vehicle applications: challenges and recommendations," *Renew. Sustain. Energy Rev.*, vol. 78, pp. 834–854, 2017.

[4] K. K. Duru, C. Karra, P. Venkatachalam, S. A. Betha, A. Anish Madhavan, and S. Kalluri, "Critical insights into fast charging techniques for lithium-ion batteries in electric vehicles," *IEEE Trans. Device Mater. Reliab.*, vol. 21, no. 1, pp. 137–152, 2021.

[5] M. Shafiei and A. Ghasemi-Marzbali, "Fast-charging station for electric vehicles, challenges and issues: a comprehensive review," *J. Energy Storage*, vol. 49, p. 104136, 2022.

[6] O. Capron, J. Jaguemont, R. Gopalakrishnan, P. Van den Bossche, N. Omar, and J. Van Mierlo, "Impact of the temperature in the evaluation of battery performances during long-term cycling-characterisation and modelling," *Appl. Sci.*, vol. 8, no. 8, pp. 1–25, 2018.

[7] W. Li, H. Zhang, B. van Vlijmen, P. Dechent, and D. U. Sauer, "Forecasting battery capacity and power degradation with multi-task learning," *Energy Storage Mater.*, vol. 53, pp. 453–466, 2022.

[8] X. Lai et al., "Critical review of life cycle assessment of lithium-ion batteries for electric vehicles: a lifespan perspective," *eTransportation*, vol. 12, p. 100169, 2022.

[9] A. Guha and A. Patra, "State of health estimation of lithium-ion batteries using capacity fade and internal resistance growth models," *IEEE Trans. Transp. Electrif.*, vol. 4, no. 1, pp. 135–146, 2017.

[10] S. K. Thakuri, H. Li, D. Ruan, and X. Wu, "The RUL prediction of Li-Ion batteries based on adaptive LSTM." *J. Dyn. Monitoring Diagnostics*, vol. 4, no. 1, pp. 53–64, 2025.

[11] Y. Li et al., "Battery eruption triggered by plated lithium on an anode during thermal runaway after fast charging," *Energy*, vol. 239, p. 122097, 2022.

[12] W. Q. Walker et al., "The effect of cell geometry and trigger method on the risks associated with thermal runaway of lithium-ion batteries," *J. Power Sources*, vol. 524, p. 230645, 2022.

[13] A. G. Siani, M. Mousavi Badjani, H. Rismani, and M. Saeedimoghadam, "State of health estimation of lithium-ion batteries based on the CC-CV charging curve and neural network," *IETE J. Res.*, vol. 69, pp. 2950–2963, 2021.

[14] Z. Chen, H. Zhao, Y. Zhang, S. Shen, J. Shen, and Y. Liu, "State of health estimation for lithium-ion batteries based on temperature prediction and gated recurrent unit neural network," *J. Power Sources*, vol. 521, p. 230892, 2022.

[15] N. Mohanty, N. K. Goyal, and V. N. A. Naikan, "Effect of training algorithms in accurate state of charge estimation of lithium-ion batteries using NARX model," *Int. J. Heavy Veh. Syst.*, vol. 30, no. 2, pp. 232–254, 2023.

[16] S. Yang, L. Ling, X. Li, J. Han, and S. Tong, "Industrial battery state-of-health estimation with incomplete limited data towards second-life applications," *J. Dyn. Monit. Diagnostics*, vol. 3, pp. 246–257, 2024.

[17] S. Vignesh et al., "State of health (SoH) estimation methods for second life lithium-ion battery—review and challenges," *Appl. Energy*, vol. 369, p. 123542, 2024.

[18] X. Bian, Z. Wei, J. He, F. Yan, and L. Liu, "A novel model-based voltage construction method for robust state-of-health estimation of lithium-ion batteries," *IEEE Trans. Ind. Electron.*, vol. 68, no. 12, pp. 12173–12184, 2021.

[19] T. Oji, Y. Zhou, S. Ci, F. Kang, X. Chen, and X. Liu, "Data-driven methods for battery SOH estimation: survey and a critical analysis," *IEEE Access*, vol. 9, pp. 126903–126916, 2021.

[20] X. Hu, Y. Che, X. Lin, and Z. Deng, "Health prognosis for electric vehicle battery packs: a data-driven approach," *IEEE/ASME Trans. Mechatron.*, vol. 25, no. 6, pp. 2622–2632, 2020.

[21] S. Saxena, Y. Xing, D. Kwon, and M. Pecht, "Accelerated degradation model for C-rate loading of lithium-ion batteries," *Int. J. Electr. Power Energy Syst.*, vol. 107, pp. 438–445, 2019.

[22] P. A. Christensen et al., "Risk management over the life cycle of lithium-ion batteries in electric vehicles," *Renew. Sustain. Energy Rev.*, vol. 148, p. 111240, 2021.

[23] Y. Preger et al., "Degradation of commercial lithium-ion cells as a function of chemistry and cycling conditions," *J. Electrochem. Soc.*, vol. 167, no. 12, p. 120532, 2020.

[24] K. Kumar, G. Rithvik, G. Mittal, R. Arya, T. K. Sharma, and K. Pareek, "Impact of fast charging and low-temperature cycling on lithium-ion battery health: a comparative analysis," *J. Energy Storage*, vol. 94, p. 112580, 2024.

[25] C. Han et al., "Research on safety warning characteristics of battery based on temperature and force coupling signals," *J. Energy Storage*, vol. 113, p. 115602, 2025.

[26] T. Rahman and T. Alharbi, "Exploring lithium-ion battery degradation: a concise review of critical factors, impacts, data-driven degradation estimation techniques, and sustainable directions for energy storage systems," *Batteries*, vol. 10, no. 7, p. 220, 2024.

[27] J. G. Qu, Z. Y. Jiang, and J. F. Zhang, "Investigation on lithium-ion battery degradation induced by combined effect of current rate and operating temperature during fast charging," *J. Energy Storage*, vol. 52, p. 104811, 2022.

[28] S. Greenbank and D. Howey, "Automated feature extraction and selection for data-driven models of rapid battery capacity fade and end of life," *IEEE Trans. Ind. Inf.*, vol. 18, no. 5, pp. 2965–2973, 2022.

[29] S. Atalay, M. Sheikh, A. Mariani, Y. Merla, E. Bower, and W. D. Widanage, "Theory of battery ageing in a lithium-ion battery: capacity fade, nonlinear ageing and lifetime prediction," *J. Power Sources*, vol. 478, p. 229026, 2020.

[30] G. Pozzato, A. Allam, and S. Onori, "Lithium-ion battery aging dataset based on electric vehicle real-driving profiles," *Data Br.*, vol. 41, p. 107995, 2022.

[31] R. Zhou, R. Zhu, C. G. Huang, and W. Peng, "State of health estimation for fast-charging lithium-ion battery based on incremental capacity analysis," *J. Energy Storage*, vol. 51, no. 66, p. 104560, 2022.

[32] G. dos Reis, C. Strange, M. Yadav, and S. Li, "Lithium-ion battery data and where to find it," *Energy AI*, vol. 5, p. 100081, 2021.